Computers and Chemical Engineering 147 (2021) 107255

Contents lists available at ScienceDirect

Computers and Chemical Engineering

journal homepage: www.elsevier.com/locate/compchemeng

Mechanistic modeling and parameter-adaptive nonlinear model predictive control of a microbioreactor

Moo Sun Hong, Richard D. Braatz*

Department of Chemical Engineering, Massachusetts Institute of Technology, 77 Massachusetts Avenue, Cambridge, MA 02139, USA

ARTICLE INFO

Article history:
Received 21 September 2020
Revised 2 February 2021
Accepted 3 February 2021
Available online 4 February 2021

Keywords:
Bioprocess engineering
Microbioreactor
Bioreactor control
Mechanistic modeling
Parameter adaptation
Model predictive control

ABSTRACT

Microbioreactors are a promising technology to accelerate biologic drug development. In aerobic cellular respiration, a potential limit to the productivity of such systems is the transport of oxygen from an external gas to the most oxygen-deficient cells, and the potential for excessive spatially localized dissolved oxygen which can result in cellular damage. This article analytically solves a mechanistic model for the spatiotemporal transport of oxygen through a gas-permeable membrane to the cells within a microbioreactor. An analytical solution to the partial differential equations for oxygen transport is derived using the finite Fourier transform method. A parameter-adaptive extended Kalman filter is shown to produce highly accurate estimates of the oxygen uptake rate of the cells, with some fluctuation in estimates of the specific cell growth rate and the specific oxygen uptake rate. The estimates are fed to a model predictive control formulation that improves the spatial control of dissolved oxygen during cell growth by more than 30% compared to a PID controller.

1. Introduction

Biologic drugs are products derived from biological organisms for treating or preventing diseases. With continued growth of biologic drugs, microscale technologies for high-speed process development is a trend in process development for biopharamaceutical manufacturing (Hong et al., 2018; 2020).

Conventional bench-scale stirred-tank bioreactors are well established for bioprocess development but are expensive in terms of labor and cost, especially when operated in parallel for the optimization of media and determination of optimal operating protocols during startup and transition to perfusion mode. Microbioreactor systems with embedded sensors for control and automation have been proposed as a more efficient alternative (Kim and Lee, 1998; Kostov et al., 2001). The primary fast dynamics that need to be controlled in a bioreactor in general and a microbioreactor in particular are associated with the dissolved oxygen (aka DO) concentration. DO concentration either too high or too low causes cell damage or death (Baez and Shiloach, 2014).

The conventional method of bubble sparging is not feasible for aeration at the small volumes in microbioreactors, where bubbles would cause clogging and flow disruptions. An alternative aeration method that is feasible at small volumes is to select one or more walls of the microbioreactor as a gas-permeable membrane for oxygen to diffuse through from an oxygen source (Zanzotto et al., 2004; Szita et al., 2005; Zhang et al., 2006; Lee et al., 2006). This surface aeration provides oxygen to the cells but creates an oxygen concentration gradient in the microbioreactor. Due to physical limitations with implementing the sensors, the DO concentration is only measured at the bioreactor wall opposite of the gas-permeable membrane. A data-driven model cannot be used to determine the oxygen concentration profile in the bioreactor, since that profile is not measurable in this system. This article employs a mechanistic model, involving conservation equations, kinetics, and diffusion, which is then used to estimate the oxygen concentration gradient from the variables that are measurable. The first main objective of this article is to analytically solve and validate a mechanistic model for DO concentration in the microbioreactor.

In industrial practice, the pH, temperature, and DO concentration within bioreactors are typically controlled using Proportional-Integral-Derivative (PID) controllers. Many academic studies have been published on the open- and closed-loop control of bioreactors, which include gain-scheduled, nonlinear-inverse-based, singular, adaptive, and model predictive control systems (Banga et al., 2005; Rani and Rao, 1999). Nonlinear model predictive control (NMPC) is of interest due to its ability to explicitly address dynamic nonlinearities and constraints. Among NMPC schemes, one of the earlier proposals for bioreactor control employed a nonlinear autoregressive with exogenous input model (Hong et al., 1996). Later, an adaptive NMPC strategy was evaluated in simulations

* Corresponding author.
E-mail addresses: moosun1@mit.edu (M.S. Hong), braatz@mit.edu (R.D. Braatz).

https://doi.org/10.1016/j.compchemeng.2021.107255
0098-1354/

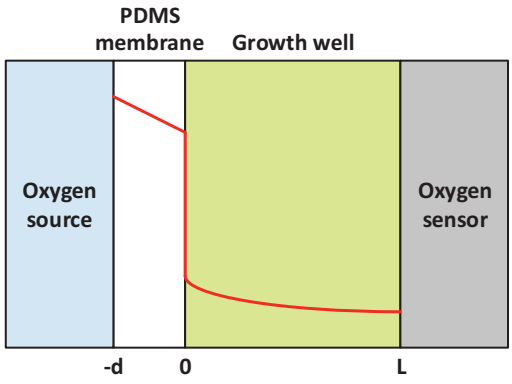

Fig. 1. Simplified model for a microbioreactor with flat form factor from Lee et al. (2006).

for the maximization of productivity of a continuous fermenter (Saha et al., 1999). Numerous later studies considered NMPC with state estimation. For example, one study investigated the potential of using NMPC with an unscented Kalman filter to control starvation-induced cell death in Chinese hamster ovary (CHO) cells in a bioreactor (Simon and Karim, 2002). Another study considered NMPC with an extended Kalman filter (EKF) for control of nitrogen and oxygen concentrations for a biological nitrogen-removal process, to make the effluent organic concentrations below regulatory limits (El Bahja et al., 2009). Very recently, an NMPC implementation that includes dynamic flux balance models was investigated for fed-batch fermentation (Chang et al., 2016). Also, NMPC has been experimentally implemented in recent years, including a study that demonstrated increased biomass and lipid productivity in a microalgal photobioreactor system (Yoo et al., 2016). The second main objective of this article is to propose and evaluate an NMPC algorithm for the control of DO concentration throughout the cell-containing spatial domain within the microbioreactor. The algorithm employs a parameter-adaptive EKF algorithm for simultaneous parameter and state estimation. The spatial variation of the DO within the microbioreactor results in different considerations than reported in the literature for stirred-tank bioreactors.

This article derives the analytical solution of a distributed parameter model for the oxygen concentration profile within the microbioreactor (Section 3), compares that model with traditional lumped parameter model (Section 4), and proposes a NMPC algorithm for oxygen control within the microbioreactor (Section 5).

2. Theory and methods

2.1. Mechanistic model

The specific microbioreactor system that served as the basis for the mathematical model is the device invented by Lee et al. (2006). The microbioreactor is designed to have a flat form factor, fabricated from polydimethylsiloxane (PDMS, Dow Corning, Sylgard 184). For modeling purposes, the physical system is simplified by approximating the effect of the peristaltic oxygenating mixer with an effective diffusion coefficient (Fig. 1) (Sagues and Horsthemke, 1986; Rosenbluth et al., 1987). In Fig. 1, the depth L of the growth well is 500 microns and the thickness d of the PDMS membrane is 70 microns. The conservation equation for the DO (Lee et al., 2006) is

$$\frac{\partial C}{\partial t} = \frac{\partial}{\partial z}\left(D(z)\frac{\partial C}{\partial z}\right) - R_V(z,t), \quad -d < z < L, \ z \neq 0, \tag{1}$$

where C is the DO concentration, the first term on the right-hand side is the one-dimensional transport in the z direction characterized by an effective DO diffusion coefficient $D(z)$, and the second term is the net rate of consumption by the cells, $R_V(z,t)$. The latter two expressions are given by

$$D(z) = \begin{cases} D_p, & -d < z < 0, \\ \eta D_w, & 0 < z < L, \end{cases} \tag{2}$$

$$R_V(z,t) = \begin{cases} 0, & -d < z < 0, \\ \mathrm{OUR}(t), & 0 < z < L, \end{cases} \tag{3}$$

where the effective diffusion coefficient of DO in PDMS is $D_p = 2.14 \times 10^{-5}$ cm^2/s (Lee et al., 2006; Lu et al., 2001), the molecular diffusion coefficient of DO in aqueous solution is $D_w = 2.19 \times 10^{-5}$ cm^2/s (St-Denis and Fell, 1971), an experimentally determined diffusion enhancement factor is $\eta = 13$, and the oxygen uptake rate (OUR) term is introduced from the cellular metabolism. The diffusion enhancement factor accounts for the effects of vibrations used by the device to increase the rate of transport of DO in the microbioreactor.

The boundary condition for the PDMS membrane comes from equilibrium with the oxygen source,

$$C(-d,t) = K_p C^*(t), \tag{4}$$

where the PDMS/gas partition coefficient is $K_p = 0.9$ mM/100% Air Sat (Lee et al., 2006; Lu et al., 2001; Merkel et al., 2000) and $C^*(t)$ is the oxygen concentration of the oxygen source. For convenience, the air saturation is used as the unit for the oxygen concentration of the oxygen source, with 100% Air Sat meaning the oxygen concentration of air with an oxygen partial pressure of 0.21 atm. The boundary condition at the end of the growth well comes from the imperviousness of the oxygen sensor,

$$\frac{\partial C}{\partial z}(L,t) = 0. \tag{5}$$

At the interface, the DO concentrations are in equilibrium and the DO flux is continuous,

$$\frac{1}{K_p}C(0^-,t) = \frac{1}{K_w}C(0^+,t), \tag{6}$$

$$D_p\frac{\partial C}{\partial z}(0^-,t) = \eta D_w\frac{\partial C}{\partial z}(0^+,t), \tag{7}$$

where the water/gas partition coefficient is $K_w = 0.27$ mM/100% Air Sat (Douglas, 1964). Alternatively, (6) could be written in terms of the water/PDMS partition coefficient, $K = K_w/K_p = 0.3$.

2.2. Finite Fourier transform analysis

The transient analysis of the mass diffusion through multilayered medium with finite geometry can be solved with method of finite Fourier transform (FFT) (Ramkrishna and Amundson, 1974). The FFT method expands the solution using eigenfunctions obtained from associated self-adjoint operators.

Consider the specific Sturm-Liouville operator needed for the problem,

$$L_x = \frac{1}{w(x)}\frac{\mathrm{d}}{\mathrm{d}x}\left(p(x)\frac{\mathrm{d}}{\mathrm{d}x}\right), \quad x \in (0,1), \tag{8}$$

where $p > 0$ and $w > 0$ for $x \in (0,1)$ and p, $\mathrm{d}p/\mathrm{d}x$, and w are continuous for $x \in [0,1]$ except at a number of intermediate points $x_1, x_2, \ldots, x_n$. The inner product can be defined to be

$$\langle f, g\rangle = \int_0^1 w(x) f(x) g(x) \mathrm{d}x. \tag{9}$$

When f and g satisfy homogeneous boundary conditions at the endpoints, it can be shown that

$$\langle L_x f, g\rangle - \langle f, L_x g\rangle = \sum_{i=1}^{n}\left[p\left(\frac{\mathrm{d}f}{\mathrm{d}x}g - f\frac{\mathrm{d}g}{\mathrm{d}x}\right)\right|_{x=x_i^-}^{x=x_i^+}. \tag{10}$$

Thus operator L_x is self-adjoint when

$$f(x_i^-) = f(x_i^+), \tag{11}$$

$$p(x_i^-)\frac{\mathrm{d}f}{\mathrm{d}x}(x_i^-) = p(x_i^+)\frac{\mathrm{d}f}{\mathrm{d}x}(x_i^+), \tag{12}$$

are satisfied for both f and g. In other words, the conditions of continuity of f and $p\frac{\mathrm{d}f}{\mathrm{d}x}$, in addition to the homogeneous boundary conditions at the endpoints, are sufficient for the specific Sturm-Liouville operator with finitely discontinuous coefficients to be self-adjoint.

2.3. Mass transfer coefficient derivation

Conventional bioreactors transport oxygen in sparged bubbles into mixed liquid containing the cells. This process is typically modeled with a two-film model that assumes the liquid film controls the overall oxygen transfer rate,

$$\frac{\mathrm{d}C}{\mathrm{d}t} = k_L a(K_w C^*(t) - C) - \mathrm{OUR}(t), \tag{13}$$

where C is the concentration in the bulk liquid and $k_L a$ is the volumetric mass transfer coefficient, which is the product of the liquid mass transfer coefficient and specific surface area.

This $k_L a$ model has been applied to the microbioreactors by approximating the bulk concentration with concentration measured at the oxygen sensor (Zanzotto et al., 2004; Lee et al., 2006). By comparison with the model developed from (1), the value of $k_L a$ can be calculated from

$$k_L a = \frac{\frac{1}{L}\left[-D\frac{\partial C}{\partial z}\right|_{z=0}}{K_w C^*(t) - C(L,t)}. \tag{14}$$

Using the quasi-steady state assumption, (1) can be directly solved to give a linear concentration profile in the PDMS membrane and quadratic concentration profile in the growth well:

$$C(z,t) = \begin{cases} K_p C^*(t) - \mathrm{OUR}(t)\frac{L(d+z)}{D_p}, & -d < z < 0, \\ K_w C^*(t) - \mathrm{OUR}(t)\left(\frac{KLd}{D_p} + \frac{L^2-(L-z)^2}{2\eta D_w}\right), & 0 < z < L. \end{cases} \tag{15}$$

With this result, the quasi-steady state value of $k_L a$ is

$$k_L a = \frac{1}{\frac{KLd}{D_p} + \frac{L^2}{2\eta D_w}} = 0.108\ \mathrm{s}^{-1}. \tag{16}$$

2.4. NMPC formulation

The NMPC algorithm repeatedly solves an online optimization based on a nonlinear process model to determine the control inputs (Henson and Seborg, 1997; Allgöwer and Zheng, 2000; Nagy and Braatz, 2010). At each sampling time, the model is updated with measurements and estimated states and the control inputs are determined over a finite prediction horizon by objective function. After the control inputs are implemented for that sampling time, the same steps are repeated by shifting the prediction horizon.

The discrete-time formulation of the optimal control problem in NMPC is usually

$$\min_{u(t_k),\ldots,u(t_{k+N_p-1})} H(x(t_k), u(t_k), \ldots, u(t_{k+N_p-1}); \theta) \tag{17}$$

with

$$x(t_{k+1}) = f(x(t_k), u(t_k); \theta), \tag{18}$$

$$y(t_k) = g(x(t_k); \theta), \tag{19}$$

$$x(t_k) = \hat{x}(t_k), \tag{20}$$

$$h(x(t_k), u(t_k), \ldots, u(t_{k+N_p-1}); \theta) \le 0, \tag{21}$$

where H is the objective function, t_k is the time at sampling time k, N_p is the prediction horizon, x is the vector of states, u is the vector of inputs, θ is the vector of parameters, y is the vector of measured variables used to compute estimated states $\hat{x}$, and h is the vector of functions describing the constraints for the system.

The states can be estimated with parameter-adaptive EKF to increase the robustness in performance of the NMPC algorithm by estimating some parameters together with the states (Maybeck, 1982; Valappil and Georgakis, 2000; Nagy and Braatz, 2010). Let $\theta' \subseteq \theta$ be the vector of estimated parameters and $\theta'' \equiv \theta \backslash \theta'$ be the vector for remaining parameters. Then the vector of augmented states is $X = [x \ \ \theta']^\top$ and the time update for the augmented states is from

$$\hat{X}^-(t_k) = \left[f(\hat{X}(t_{k-1}), u(t_{k-1}); \theta'') \ \ \theta'(t_{k-1})\right]^\top. \tag{22}$$

The time update of the state covariance is from

$$\mathbf{P}^-(t_k) = \mathbf{F}(t_{k-1})\mathbf{P}(t_{k-1})\mathbf{F}^\top(t_{k-1}) + \mathbf{Q}(t_k), \tag{23}$$

$$\mathbf{F}(t_{k-1}) = \begin{bmatrix} \frac{\partial f(\hat{X}(t_{k-1}), u(t_{k-1}); \theta'')}{\partial x} & \frac{\partial f(\hat{X}(t_{k-1}), u(t_{k-1}); \theta'')}{\partial \theta'} \\ 0 & \mathbf{I} \end{bmatrix}, \tag{24}$$

where $\mathbf{F}$ is the Jacobian given by (24) and $\mathbf{Q}$ is the process noise covariance matrix. Assuming that the process noise is mostly from the parameter uncertainty, $\mathbf{Q}$ is given by

$$\mathbf{Q}(t_k) = \begin{bmatrix} \mathbf{S}_{\theta''}(t_{k-1})\mathbf{V}_{\theta''}\mathbf{S}_{\theta''}^\top(t_{k-1}) & 0 \\ 0 & \mathbf{V}_{\theta'} \end{bmatrix}, \tag{25}$$

$$\mathbf{S}_{\theta''}(t_{k-1}) = \frac{\partial f(\hat{X}(t_{k-1}), u(t_{k-1}); \hat{\theta}'')}{\partial \theta''}, \tag{26}$$

where $\mathbf{V}_{\theta'}$ and $\mathbf{V}_{\theta''}$ are the parameter covariance matrices, $\mathbf{S}_{\theta''}$ is the Jacobian given by (26), and $\hat{\theta}''$ is the nominal parameter vector. The Kalman gain $\mathbf{K}$ is computed from

$$\mathbf{K}(t_k) = \mathbf{P}^-(t_k)\mathbf{G}(t_k)(\mathbf{G}(t_k)\mathbf{P}^-(t_k)\mathbf{G}^\top(t_k) + \mathbf{R})^{-1}, \tag{27}$$

$$\mathbf{G}(t_k) = \left[\frac{\partial g(\hat{X}^-(t_k); \theta'')}{\partial x} \ \ \frac{\partial g(\hat{X}^-(t_k); \theta'')}{\partial \theta'}\right], \tag{28}$$

where $\mathbf{G}$ is the Jacobian given by (28) and $\mathbf{R}$ is the measurement noise covariance matrix. Finally, the measurement update is computed from

$$\hat{X}(t_k) = \hat{X}^-(t_k) + \mathbf{K}(t_k)(y(t_k) - g(\hat{X}^-(t_k); \theta'')), \tag{29}$$

$$\mathbf{P}(t_k) = (\mathbf{I} - \mathbf{K}(t_k)\mathbf{G}(t_k))\mathbf{P}^-(t_k). \tag{30}$$

3. Analytical solution of the microbioreactor model

For convenience, new variables are introduced for the length and concentration,

$$x = \frac{z+d}{L+d}, \quad \Theta = \frac{C}{K(x)}. \tag{31}$$

With the location of the interface expressed as $\gamma = \frac{d}{L+d}$, $K(x)$ is the partition coefficient for PDMS/gas $(0 < x < \gamma)$ or water/gas

($\gamma < x < 1$). The model equations with boundary and interface conditions are rewritten in terms of new variables as

$$\frac{\partial \Theta}{\partial t} = \frac{1}{K(x)} \frac{\partial}{\partial x}\left(K(x)\tilde{D}(x)\frac{\partial \Theta}{\partial x}\right) + \tilde{R}_V(x,t), \tag{32}$$

$$\tilde{D}(x) = \begin{cases} \tilde{D}_p = \frac{D_p}{(L+d)^2}, & 0 < x < \gamma, \\ \tilde{D}_w = \frac{\eta D_w}{(L+d)^2}, & \gamma < x < 1, \end{cases} \tag{33}$$

$$\tilde{R}_V(x,t) = \begin{cases} 0, & 0 < x < \gamma, \\ \frac{\mathrm{OUR}(t)}{K_w}, & \gamma < x < 1, \end{cases} \tag{34}$$

$$\Theta(0,t) = C^*(t), \quad \frac{\partial \Theta}{\partial x}(1,t) = 0, \tag{35}$$

$$\Theta(\gamma^-,t) = \Theta(\gamma^+,t), \quad K_p\tilde{D}_p\frac{\partial \Theta}{\partial x}(\gamma^-,t) = K_w\tilde{D}_w\frac{\partial \Theta}{\partial x}(\gamma^+,t). \tag{36}$$

The analytical solution to this partial differential equation with two spatial domains,

$$\Theta(x,t) = \sum_{n=1}^{\infty} \Theta_n(t)\Phi_n(x), \tag{37}$$

can be derived for this problem by application of the FFT method (Ramkrishna and Amundson, 1974), where

$$\Phi_n(x) = \begin{cases} A_{p,n}\sin\frac{\lambda_n x}{\sqrt{\tilde{D}_p}}, & 0 < x < \gamma, \\ A_{w,n}\sin\frac{\lambda_n x}{\sqrt{\tilde{D}_w}} + B_{w,n}\cos\frac{\lambda_n x}{\sqrt{\tilde{D}_w}}, & \gamma < x < 1, \end{cases} \tag{38}$$

$$A_{w,n} = \frac{1}{\sqrt{K_p N_{\lambda_n}}}, \; B_{w,n} = -\frac{M_{\lambda_n,21}}{M_{\lambda_n,22}}\frac{1}{\sqrt{K_p N_{\lambda_n}}}, \; A_{p,n} = \frac{\left|\mathbf{M}_{\lambda_n}\right|}{M_{\lambda_n,22}}\frac{1}{\sqrt{K_p N_{\lambda_n}}}, \tag{39}$$

$$\Theta_n(t) = \left(\Theta_n(0) + B_n\int_0^t C^*(\tau)e^{\lambda_n^2\tau}\mathrm{d}\tau - R_n\int_0^t \mathrm{OUR}(\tau)e^{\lambda_n^2\tau}\mathrm{d}\tau\right)e^{-\lambda_n^2 t}, \tag{40}$$

for $n = 1, 2, \ldots$ (see Supplementary Material for details).

4. Dissolved oxygen concentration profiles

This section examines the concentration profiles obtained from the FFT model to determine the applicability of the k_La model to the microbioreactor. The k_La value for the model is taken from (16), which matches the dynamic gassing measurements from Lee et al. (2006). To determine the concentration profiles from the FFT model and k_La models, the oxygen concentration in the oxygen source ($C^*(t)$) and the oxygen uptake rate (OUR) must be specified. The oxygen source is from the reservoir that mixes input pure oxygen and air. These input gases are fed to the reservoir with constant overall flow rate but with different ratio determined by the controller. The concentration of the oxygen source can be modeled by

$$\frac{\mathrm{d}C^*}{\mathrm{d}t} = \frac{F}{V}(C_{\mathrm{in}} - C^*), \tag{41}$$

where the flow rate F is 3.9 L/h, the volume of the reservoir V is 0.75 mL, and C_{in} is the concentration of input gas determined by the ratio of pure oxygen and air. Solving (41) while the ratio is fixed between the control actions gives the concentration of oxygen source as

$$C^*(t) = C_{\mathrm{in}} + (C^*(0) - C_{\mathrm{in}})e^{-Ft/V}. \tag{42}$$

An oxygen uptake rate with constant specific oxygen uptake rate ($q_O = 20$ mmol/g/h) (Andersen and von Meyenburg, 1980) and constant specific growth rate ($\mu = 0.5$ h^{-1}) (Li et al., 1992) is represented as

$$\mathrm{OUR}(t) = q_O X(t) = q_O X(0)e^{\mu t}, \tag{43}$$

where $X(t)$ is the cell density as function of time, which has exponential growth. With these conditions, (40) can be written as

$$\Theta_n(t) = \Theta_n(0)e^{-\lambda_n^2 t} + B_n\left(\frac{C_{\mathrm{in}}}{\lambda_n^2}\left(1 - e^{-\lambda_n^2 t}\right) + \frac{C^*(0) - C_{\mathrm{in}}}{\lambda_n^2 - F/V}\left(e^{-Ft/V} - e^{-\lambda_n^2 t}\right)\right) - \frac{R_n q_O X(0)}{\lambda_n^2 + \mu}\left(e^{\mu t} - e^{-\lambda_n^2 t}\right). \tag{44}$$

This expression suggests a superposition of the form,

$$\Theta(x,t) = C_{\mathrm{in}}p(x) + (C^*(0) - C_{\mathrm{in}})e^{-Ft/V}q(x) + \Psi(x,t). \tag{45}$$

With this form of the solution, $\Psi(x,t)$ now satisfies homogeneous boundary conditions, allowing the concentration to be differentiable and the flux to be determined for the k_La calculation. The newly introduced functions can be evaluated by

$$\frac{\mathrm{d}^2 p}{\mathrm{d}x^2} = 0, \quad p(0) = 1, \quad \frac{\mathrm{d}p}{\mathrm{d}x}(1) = 0, \tag{46}$$

$$\frac{\mathrm{d}^2 q}{\mathrm{d}x^2} + \frac{F}{V}\frac{1}{\tilde{D}}q = 0, \quad q(0) = 1, \quad \frac{\mathrm{d}q}{\mathrm{d}q}(1) = 0, \tag{47}$$

$$q(\gamma^-) = q(\gamma^+), \quad K_p\tilde{D}_p\frac{\mathrm{d}q}{\mathrm{d}x}(\gamma^-) = K_w\tilde{D}_w\frac{\mathrm{d}q}{\mathrm{d}x}(\gamma^+). \tag{48}$$

Solving these equations results in

$$p(x) = 1, \tag{49}$$

$$q(x) = \begin{cases} A_{p,q}\sin\left(x\sqrt{\frac{F}{V}\frac{1}{\tilde{D}_p}}\right) + B_{p,q}\cos\left(x\sqrt{\frac{F}{V}\frac{1}{\tilde{D}_p}}\right), & 0 < x < \gamma, \\ A_{w,q}\sin\left(x\sqrt{\frac{F}{V}\frac{1}{\tilde{D}_w}}\right) + B_{w,q}\cos\left(x\sqrt{\frac{F}{V}\frac{1}{\tilde{D}_w}}\right), & \gamma < x < 1, \end{cases} \tag{50}$$

where

$$\begin{bmatrix} A_{p,q} \\ B_{p,q} \end{bmatrix} = \mathbf{M}_{FV}\begin{bmatrix} A_{w,q} \\ B_{w,q} \end{bmatrix} = \begin{bmatrix} M_{FV,11} & M_{FV,12} \\ M_{FV,21} & M_{FV,22} \end{bmatrix}\begin{bmatrix} A_{w,q} \\ B_{w,q} \end{bmatrix}, \tag{51}$$

$$A_{p,q} = \frac{M_{FV,11}\tan\sqrt{\frac{F}{V}\frac{1}{\tilde{D}_w}} + M_{FV,12}}{M_{FV,21}\tan\sqrt{\frac{F}{V}\frac{1}{\tilde{D}_w}} + M_{FV,22}}, \quad B_{p,q} = 1, \tag{52}$$

$$A_{w,q} = \frac{\tan\sqrt{\frac{F}{V}\frac{1}{\tilde{D}_w}}}{M_{FV,21}\tan\sqrt{\frac{F}{V}\frac{1}{\tilde{D}_w}} + M_{FV,22}}, \quad B_{w,q} = \frac{1}{M_{FV,21}\tan\sqrt{\frac{F}{V}\frac{1}{\tilde{D}_w}} + M_{FV,22}}. \tag{53}$$

The FFT method can be used to solve for $\Psi(x,t)$ using the same eigenfunctions given by (38),

$$\Psi(x,t) = \sum_{n=1}^{\infty} \Psi_n(t)\Phi_n(x), \tag{54}$$

$$\Psi_n(t) = \Psi_n(0)e^{-\lambda_n^2 t} - \frac{R_n q_O X(0)}{\lambda_n^2 + \mu}\left(e^{\mu t} - e^{-\lambda_n^2 t}\right). \tag{55}$$

Compared to (44), the B_n term is zero due to the homogeneous boundary condition. The last undetermined term $\Psi_n(0)$ can be determined from the initial condition. A constant concentration

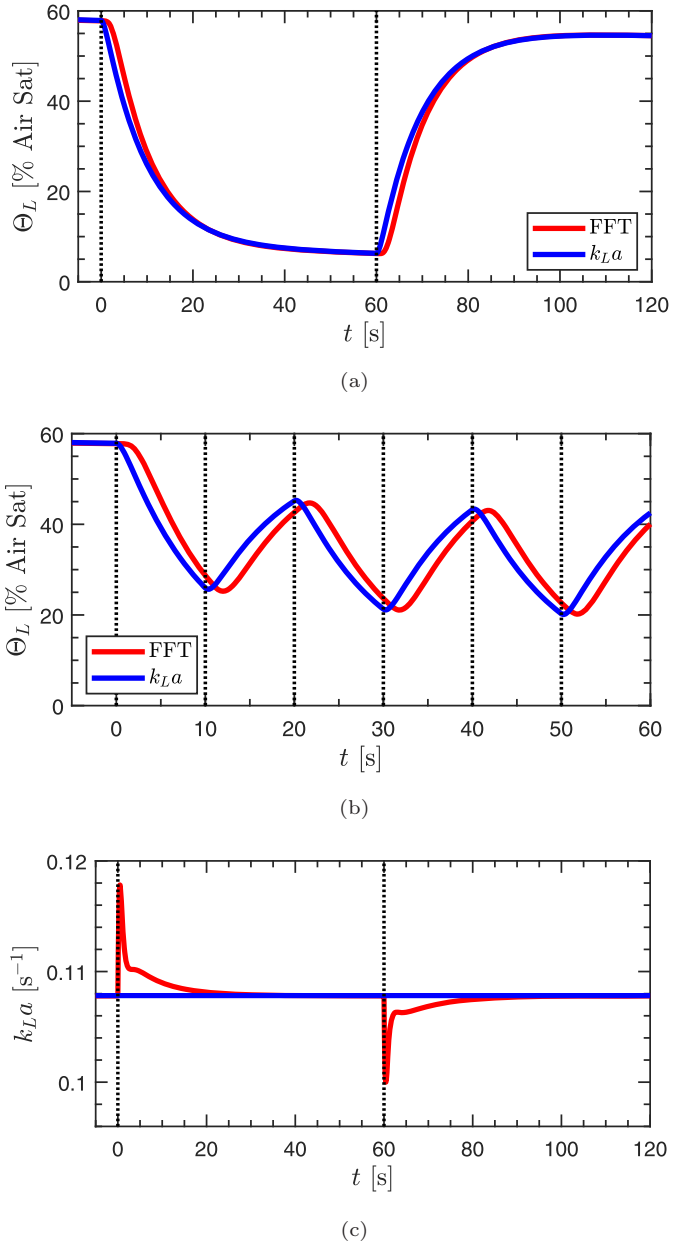

Fig. 2. Transient responses of the dissolved oxygen concentration at the oxygen sensor for the k_La and FFT models in response to (a) step changes made every 60 s and (b) step changes made every 10 s. (c) Transient responses of the mass transfer coefficient k_La calculated from (14) with the FFT model (red line) and quasi-steady state value (16) used in the k_La model (blue line) for step changes made every 60 s. (For interpretation of the references to color in this figure legend, the reader is referred to the web version of this article.)

profile in equilibrium with the oxygen source as the initial condition results in

$$\Psi(x,0) = (C^*(0) - C_{\text{in}})(1 - q(x)), \tag{56}$$

$$\Psi_n(0) = \langle \Psi(x,0), \Phi_n \rangle = B_n(C^*(0) - C_{\text{in}})\left(\frac{1}{\lambda_n^2} - \frac{1}{\lambda_n^2 - F/V}\right). \tag{57}$$

The final concentration profile at the previous control action as the initial condition results in

$$\Psi(x,0) = C_{\text{in},p} + \left(C_p^*(0) - C_{\text{in},p}\right)e^{-Ft/V}q(x) + \sum_{n=1}^{\infty}\Psi_{n,p}(T)\Phi_n(x) - C_{\text{in}} - (C^*(0) - C_{\text{in}})q(x), \tag{58}$$

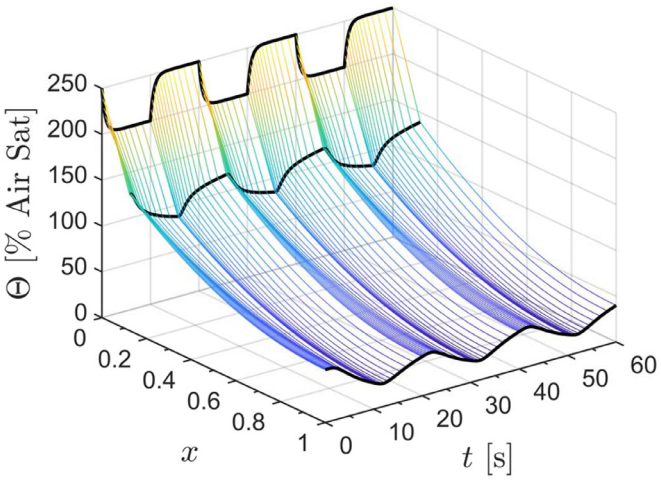

Fig. 3. Concentration profile throughout the microbioreactor from the FFT model. The black lines indicate concentration at the boundaries and the interface.

$$\Psi_n(0) = \langle \Psi(x,0), \Phi_n \rangle = \Psi_{n,p}(T) + \frac{B_n}{\lambda_n^2}\left(C_{\text{in},p} - C_{\text{in}}\right) + \frac{B_n}{\lambda_n^2 - F/V}\left(\left(C_p^*(0) - C_{\text{in},p}\right)e^{-Ft/V} + C^*(0) - C_{\text{in}}\right) \tag{59}$$

where the subscript p represents the values from the last control action and T is the time period of the control action. The concentration profile is then given by (38), (45), (49), (50), (54), (55), (57), and (59).

The k_La and FFT models are evaluated by simulating step changes in the input gas concentration. The system is initially at quasi-steady state with 250% Air Sat input gas, then the input gas concentration is alternated between 200 and 250% Air Sat.

Fig. 2a shows the concentrations at the oxygen sensor for each model when the concentration of input gas is alternated every 60 s. The k_La and FFT models overlap as quasi-steady state is approached, with difference less than 1% Air Sat after ~15 s (0.2% Air Sat after ~20 s). That is, the models agree when the time after the step change is a factor of about two larger than the characteristic time for the DO transport, on the order of $1/k_La \approx 10$ s.

The transient behaviors after the step changes, however, are different for the two models. Fig. 2b shows the difference when the input gas concentration is alternated every 10 s. The DO concentration at the oxygen sensor responds more quickly to the step changes for the k_La model. Because the k_La model is a lumped parameter model with constant quasi-steady state k_La value, the change in the concentration of the oxygen source caused by the step change is sensed instantaneously, leading to immediate response of the oxygen transfer rate and the DO concentration at the oxygen sensor in sequence. The k_La value calculated from (14) with the FFT model shows that the actual k_La value is not constant but varies rapidly after the step change to counteract the change in the concentration gradient due to concentration of oxygen source (Fig. 2c).

In addition to the inaccurate transient behaviors after the step change, the k_La model is not able to capture the actual concentration profile in the microbioreactor, especially in the growth well. The concentration profile varies over time due to the step change in the input gas concentration and the exponentially increasing oxygen uptake rate (Fig. 3). The significant difference in the concentration throughout the growth well is evident for the high oxygen uptake rate occurring at experimental conditions. The DO concentration at the oxygen sensor, which is the only concentration available in the actual experimental setup, can only serve as the minimum concentration in the growth well.

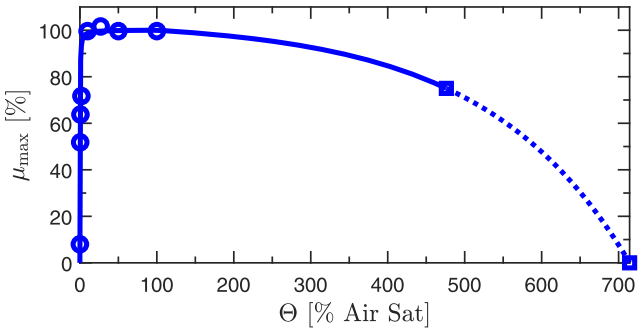

Fig. 4. Specific growth rate measurements from Li et al. (1992) (circles) and Brunker and Brown (1971) (squares) and the exponentially decreasing specific growth rate model constructed from the measurements (line).

5. Feedback control results

The DO concentration profile provided from the FFT model is important in terms of DO control in the microbioreactor. Oxygen toxicity is well-known to occur when the DO concentration is excessive (Fridovich, 1998). As such, the classical PID control strategy of controlling the DO concentration at the oxygen sensor is not ideal. A better strategy is to control the DO concentration throughout the growth well using NMPC. NMPC can explicitly take into the effect of DO concentration on the cell metabolism such as growth and production that directly impacts the time and cost for the manufacturing.

The cell type in the microbioreactor used for the experiments was *Escherichia coli*, which is one of the most widely used bacteria species in the bioprocess industry. Because *E. coli* has been widely studied, numerous studies are available that report the effect of the DO concentration on the specific growth rate of the *E. coli*. Within the oxygen concentration of air saturation, Li et al. (1992) found that the specific growth rate increased with the DO concentration in accordance with the Monod model. Over the oxygen concentration of air saturation, Brunker and Brown (1971) found that the cultivation with pure oxygen at 1 bar decreased the specific growth rate by 25% compared to the air, whereas pure oxygen above 1.5 bar was completely bacteriostatic, inhibiting the cell growth. Here the experimental observations of these regions are described by the specific growth rate decreasing exponentially as the DO concentration increases (Fig. 4).

With this information on the dependence of specific growth rate on the DO concentration, the optimal control problem for each NMPC calculation can be formulated as minimizing the decrease in the maximum specific growth rate throughout the growth well,

$$\min_{C_{\text{in}}(t_k),\ldots,C_{\text{in}}(t_{k+N_p-1})} \sum_{i=k+1}^{k+N_p} \sum_{j=1}^{N_z} \left(1 - \frac{\mu_{\max}\big(\Theta(z_j,t_i)\big)}{\mu_{\max}(\Theta_{\max})}\right)^2, \tag{60}$$

$$\frac{\mu_{\max}(\Theta)}{\mu_{\max}(\Theta_{\max})} = \begin{cases} \frac{\Theta}{K+\Theta}\frac{K+\Theta_{\max}}{\Theta_{\max}}, & \Theta < \Theta_{\max}, \\ 1 - a\big(e^{b(\Theta-\Theta_{\max})} - 1\big), & \Theta > \Theta_{\max}, \end{cases} \tag{61}$$

where $\mu_{\max}$ is the maximum specific growth rate; $\Theta_{\max}$ is the oxygen concentration of air saturation; z_j is the length from the interface, which the length is divided with discrete steps $z_1 = 0 < z_2 < \ldots < z_j < \ldots < z_{N_z} = L$; t_i is the sampling time; and N_p is the prediction horizon. The concentration profile is predicted using the FFT model. In the actual microbioreactor, the specific oxygen uptake rate and the specific growth rate are not constants. For accurate state estimation, a parameter-adaptive EKF was incorporated into the NMPC formulation, including the specific growth rate and specific oxygen uptake rate as the estimated parameters. The process model is

$$x(t_k) = [C^*(t_k) \;\; C^*(t_{k-1}) \;\; X(t_k) \;\; \Psi_n(t_k) \;\; \Theta_L(t_k) \;\; \mu(t_k) \;\; q_O(t_k)]^\top, \tag{62}$$

$$x(t_0) = [C^*(t_0) \;\; C^*(t_0) \;\; X(t_0) \;\; 0 \;\; C^*(t_0) \;\; \mu(t_0) \;\; q_O(t_0)]^\top, \tag{63}$$

$$u(t_k) = [C_{\text{in}}(t_k) \;\; C_{\text{in}}(t_{k-1})]^\top, \tag{64}$$

$$u(t_0) = [C_{\text{in}}(t_0) \;\; C^*(t_0)]^\top, \tag{65}$$

$$\theta = [D_p \;\; \eta \;\; D_w \;\; K_p \;\; K_w]^\top, \tag{66}$$

$$x(t_{k+1}) = f(x(t_k), u(t_k); \theta) = \begin{bmatrix} C_{\text{in}}(t_k) + (C^*(t_k) - C_{\text{in}}(t_k))e^{-FT/V} \\ C^*(t_k) \\ X(t_k)e^{\mu(t_k)T} \\ \left\{\left\{\Psi_n(t_k) + \frac{B_n}{\lambda_n^2}(C_{\text{in}}(t_{k-1}) - C_{\text{in}}(t_k)) + \frac{B_n}{\lambda_n^2 - F/V}\right.\right. \\ \left.\left.\big((C^*(t_{k-1}) - C_{\text{in}}(t_{k-1}))e^{-FT/V} - (C^*(t_k) - C_{\text{in}}(t_k))\big)\right\}e^{-\lambda_n^2 T} \right. \\ \left. - \frac{R_n q_O(t_k) X(t_k)}{\lambda_n^2 + \mu(t_k)}\big(e^{\mu(t_k)T} - e^{-\lambda_n^2 T}\big)\right\} \\ C_{\text{in}}(t_k) + (C^*(t_k) - C_{\text{in}}(t_k))q(L)e^{-FT/V} + \sum_n \Psi_n(t_{k+1})\Phi_n(L) \\ \mu(t_k) \\ q_O(t_k) \end{bmatrix} \tag{67}$$

$$y(t_k) = g(x(t_k); \theta) = [X(t_k) \;\; \Theta_L(t_k)]^\top, \tag{68}$$

where Θ_L is the concentration at the oxygen sensor and θ is the vector of model parameters with hyperellipsoidal parameter uncertainty described by the covariance matrix.

The parameter covariances are based on experimental values (Douglas, 1964; St-Denis and Fell, 1971; Merkel et al., 2000; Lu et al., 2001) and their dependence on the temperature and growth media compositions can be described by

$$\theta_i = \hat{\theta}_i + a_{T,i} w_T + a_{G,i} w_G + w_{M,i}, \tag{69}$$

$$\text{var}(\theta_i) = a_{T,i}^2 \sigma_T^2 + a_{G,i}^2 \sigma_G^2 + \sigma_{M,i}^2 = \sigma_{\theta_i}^2, \tag{70}$$

$$\text{cov}(\theta_i, \theta_j) = a_{T,i} a_{T,j} \sigma_T^2 + a_{G,i} a_{G,j} \sigma_G^2, \tag{71}$$

where w_T, w_G, and w_M are zero-mean Gaussian white-noise variables of temperature, growth media compositions, and measurement error; and a_T and a_G are coefficients showing the dependence of the parameters on the temperature and growth media compositions (Table 1). The control input is the input gas concentration and the measured variables are the cell density and the DO concentration at the oxygen sensor.

The NMPC is compared to the original PID control in simulations, assuming random measurement noise with standard deviation of 1 g-dry cell weight (DCW)/L for the cell density and 3%

Table 1
Values assumed for the parameter covariances.

θ_i	D_p	ηD_w	K_p	K_w
$a_{T,i}\sigma_T/\hat{\theta}_i$	0.02	0.02	−0.02	−0.02
$a_{G,i}\sigma_G/\hat{\theta}_i$	0	−0.03	0	−0.03
$\sigma_{\theta_i}/\hat{\theta}_i$	0.05	0.05	0.05	0.05

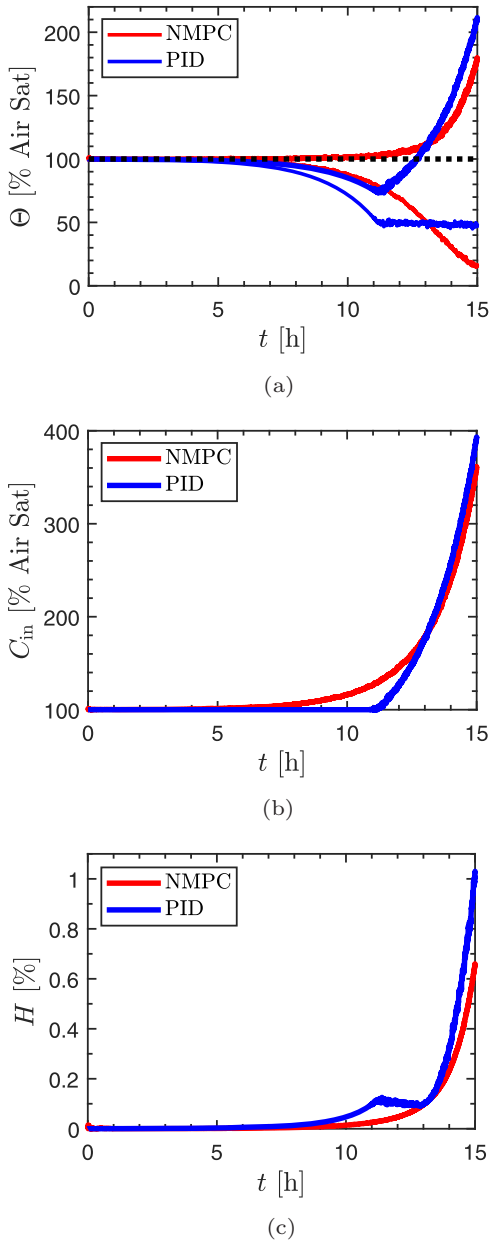

Fig. 5. (a) DO concentrations at the sensor and the interface, (b) input gas concentrations, and (c) quadratic mean of decrease in the maximum specific growth rate for NMPC and PID control. (For interpretation of the references to color in this figure legend, the reader is referred to the web version of this article.)

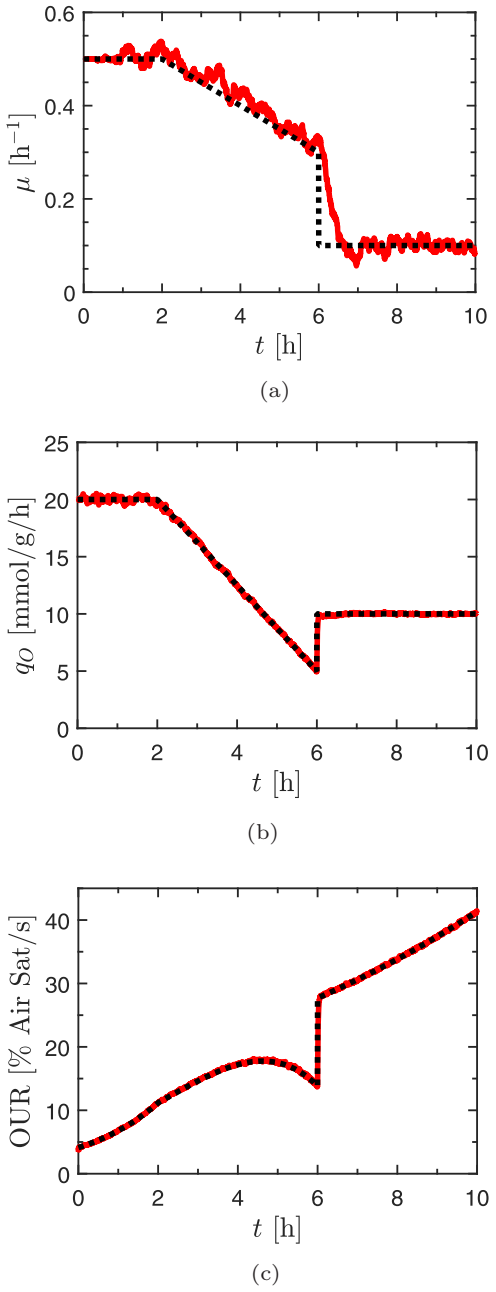

Fig. 6. On-line estimates of the (a) specific growth rate, (b) specific oxygen uptake rate, and (c) oxygen uptake rate obtained by the parameter-adaptive EKF (solid lines) with $\sigma_\mu = 0.005\mu$ and $\sigma_{q_o} = 0.005q_O$ compared to the actual values (dotted lines). The estimation errors of the specific growth rate and the specific oxygen uptake rate decrease as the number of cells in the microbioreactor increase and overall take up oxygen at a higher rate.

Air Sat for the DO concentration at each sampling instance. The setpoint for the PID control was set to 50% Air Sat and the sampling period was set to 10 s. The numerical algorithms were implemented in Matlab and are available for download (Hong and Braatz, 2021). The NMPC Matlab code can be experimentally implemented on the physical system by using the Matlab Instrument Control Toolbox to swap the simulation model with the experimental system in the Matlab code.

Fig. 5a and b show the temporal response in the DO concentrations at the sensor and the interface with the input gas concentration set by NMPC and PID control. The NMPC shows an interesting manipulation of input gas concentration compared to PID control. Initially, while the oxygen uptake rate is still low, NMPC chose higher input gas concentration than PID control, to minimize its objective by maintaining the oxygen concentration profile around the air saturation. As the oxygen uptake rate increases, the DO concentration profile through the growth well widens (Fig. 5a) and higher DO concentrations affect the specific growth rate more negatively compared to the lower concentration. As such, the input gas concentration chosen by NMPC becomes lower than that of PID control, allowing the DO concentration at the sensor to be lower than the setpoint of the PID controller.

The NMPC formulation incorporates parameter estimation for the specific growth rate and the specific oxygen uptake rate, which determine the cell density and the oxygen uptake rate. The parameter estimation removes the needs for an accurate model of the cell metabolism, which allows the NMPC to be widely applied to

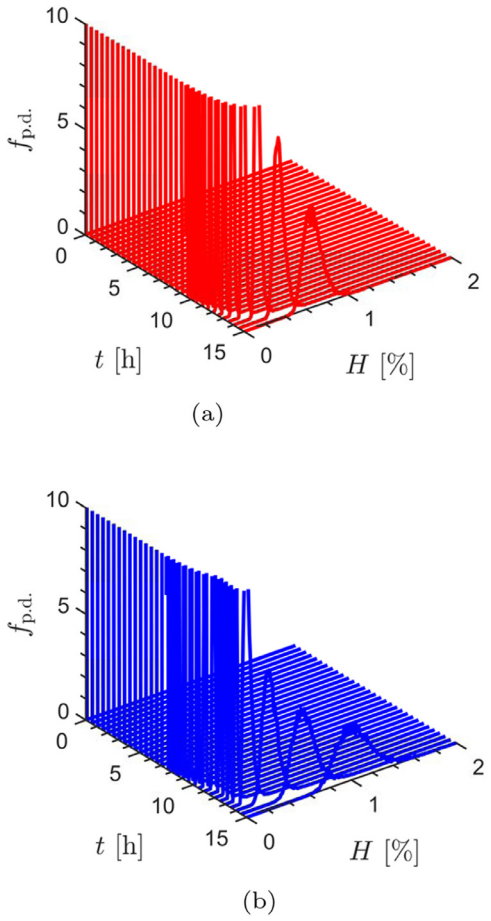

Fig. 7. Time variation of the probability distribution functions of the quadratic mean of decrease in the specific growth rate for (a) NMPC and (b) PID control. The probability distribution functions were determined from Monte Carlo simulations.

different cells and operation modes. Fig. 6 plot the estimates of the specific growth rate, specific oxygen uptake rate, and oxygen uptake rate to a linear and step change in the actual value of specific growth rate and specific oxygen uptake rate. The estimated specific growth rate and specific oxygen uptake rate converge to the actual value with some fluctuations, while the estimated oxygen uptake rate tightly tracks the true value over whole time period. For the low cell density and oxygen uptake rate during the initial period, changes in cell density and DO concentration are comparable to the measurement noise. The parameter estimation can be improved to track the actual value faster by increasing the variance of the specific growth rate and the specific oxygen uptake rate fed to the parameter-adaptive EKF, but that tuning would make the parameter estimation more sensitive to the measurement noise and amplify the fluctuations.

Fig. 5c shows the temporal response for the value of the quadratic mean of decrease in the maximum specific growth rate,

$$H(t) = \sqrt{\frac{1}{N_z}\sum_{j=1}^{N_z}\left[1 - \frac{\mu_{\max}\left(\Theta(z_j,t)\right)}{\mu_{\max}(\Theta_{\max})}\right]^2}, \tag{72}$$

for both NMPC and PID control. NMPC results in about a 35% decrease in the value of H at the end of the simulation time compared to PID control. The NMPC formulation provided optimal control of the microbioreactor for the given objective. The objective was growth rate for this study but this can be further extended to other important characteristics such as productivity and viability. NMPC would have greater value for eukaryotes, such as the CHO cells widely used to make monoclonal antibodies and other biopharmaceuticals, because they are more sensitive to the oxygen concentration than the *E. coli* used in this study.

To investigate the effect of the parameter uncertainty in the model, the value of H was computed using Monte Carlo simulation with 10,000 random parameter sets obtained from the covariance matrix, and used to construct the probability distribution functions in Fig. 7. The variance of H obtained by NMPC is smaller than that of PID control, by about 70% at the end of the simulation time. The NMPC formulation is more robust to the parameter uncertainties, including those not explicitly considered in the state estimation.

6. Conclusion

This article derives the analytical solution of a mechanistic model for the transient oxygen concentration profile throughout a microbioreactor using the FFT method. The simulation results show the limitation of the k_La model in capturing transient behavior and the concentration profile throughout the growth well. A parameter-adaptive EFK-based NMPC algorithm was proposed to replace PID control for the DO concentration to minimize the effect of the oxygen concentration profile throughout the growth well on the maximum specific cell growth rate. The estimation of specific growth rate and specific oxygen uptake rate with cell density and DO concentration measurement enables the NMPC to be applicable to various microbioreactor systems with different cells and operation modes.

Declaration of Competing Interest

The authors declare that they have no known competing financial interests or personal relationships that could have appeared to influence the work reported in this paper.

CRediT authorship contribution statement

Moo Sun Hong: Conceptualization, Methodology, Formal analysis, Investigation, Writing - original draft, Writing - review & editing. **Richard D. Braatz:** Conceptualization, Writing - original draft, Writing - review & editing, Funding acquisition.

Acknowledgment

This material is based upon work supported in part by the Defense Advanced Research Projects Agency (DARPA) and SPAWAR Systems Center Pacific (SSC Pacific) under Contract No. N66001-13-C-4025. Any opinions, findings and conclusions or recommendations expressed in this material are those of the author(s) and do not necessarily reflect the views of the Defense Advanced Research Projects Agency (DARPA) and SPAWAR Systems Center Pacific (SSC Pacific).

Supplementary material

Supplementary material associated with this article can be found, in the online version, at doi:10.1016/j.compchemeng.2021.107255.

References

Allgöwer, F., Zheng, A. (Eds.), 2000. Nonlinear Model Predictive Control. Birkhäuser, Basel, Switzerland.

Andersen, K.B., von Meyenburg, K., 1980. Are growth rates of Escherichia coli in batch cultures limited by respiration? J. Bacteriol. 144 (1), 114–123.

Baez, A., Shiloach, J., 2014. Effect of elevated oxygen concentration on bacteria, yeasts, and cells propagated for production of biological compounds. Microb. Cell Fact. 13 (1), 181. doi:10.1186/s12934-014-0181-5.

Banga, J.R., Balsa-Canto, E., Moles, C.G., Alonso, A.A., 2005. Dynamic optimization of bioprocesses: efficient and robust numerical strategies. J. Biotechnol. 117 (4), 407–419. doi:10.1016/j.jbiotec.2005.02.013.

Brunker, R.L., Brown, O.R., 1971. Effects of hyperoxia on oxidized and reduced NAD and NADP concentrations in Escherichia coli. Microbios. 4 (15), 193–203.

Chang, L., Liu, X., Henson, M.A., 2016. Nonlinear model predictive control of fed-batch fermentations using dynamic flux balance models. J. Process Contr. 42, 137–149. doi:10.1016/j.jprocont.2016.04.012.

Douglas, E., 1964. Solubilities of oxygen, argon, and nitrogen in distilled water. J. Phys. Chem. 68 (1), 169–174. doi:10.1021/j100783a028.

El Bahja, H., Vega, P., Bakka, O., Mesquine, F., 2009. Non linear GPC of a nutrient removal biological plant. In: 2009 IEEE Conference on Emerging Technologies & Factory Automation, pp. 1–7. doi:10.1109/ETFA.2009.5347099.

Fridovich, I., 1998. Oxygen toxicity: a radical explanation. J. Exp. Biol. 201 (8), 1203–1209.

Henson, M.A., Seborg, D.E. (Eds.), 1997. Nonlinear Process Control. Prentice Hall PTR, Upper Saddle River, NJ.

Hong, M.S., Braatz, R.D., 2021. Mechanistic Modeling and Parameter-Adaptive Nonlinear Model Predictive Control of a Microbioreactor. Massachusetts Institute of Technology, Cambridge, MA. Software. Available for download at https://web.mit.edu/braatzgroup/MicrobioreactorHong.zip

Hong, M.S., Severson, K.A., Jiang, M., Lu, A.E., Love, J.C., Braatz, R.D., 2018. Challenges and opportunities in biopharmaceutical manufacturing control. Comput. Chem. Eng 110, 106–114. doi:10.1016/j.compchemeng.2017.12.007.

Hong, M.S., Sun, W., Lu, A.E., Braatz, R.D., 2020. Process analytical technology and digital biomanufacturing of monoclonal antibodies. Am. Pharm. Rev. 23 (6), 122–125.

Hong, T., Zhang, J., Morris, A.J., Martin, E.B., Karim, M.N., 1996. Neural based predictive control of a multivariable microalgae fermentation. In: 1996 IEEE International Conference on Systems, Man and Cybernetics. Information Intelligence and Systems, Vol. 1, pp. 345–350. doi:10.1109/ICSMC.1996.569793.

Kim, J.W., Lee, Y.H., 1998. Development of microfermenter chip. J. Korean Phys. Soc. 33, S462–S466.

Kostov, Y., Harms, P., Randers-Eichhorn, L., Rao, G., 2001. Low-cost microbioreactor for high-throughput bioprocessing. Biotechnol. Bioeng. 72 (3), 346–352. doi:10.1002/1097-0290(20010205)72:3<346::AID-BIT12>3.0.CO;2-X.

Lee, H.L.T., Boccazzi, P., Ram, R.J., Sinskey, A.J., 2006. Microbioreactor arrays with integrated mixers and fluid injectors for high-throughput experimentation with pH and dissolved oxygen control. Lab Chip 6 (9), 1229–1235. doi:10.1039/B608014F.

Li, X., Robbins, J.W., Taylor, K.B., 1992. Effect of the levels of dissolved oxygen on the expression of recombinant proteins in four recombinant Escherichia coli strains. J. Ind. Microbiol. Biot. 9 (1), 1–9. doi:10.1007/BF01576362.

Lu, X., Manners, I., Winnik, M.A., 2001. Polymer/silica composite films as luminescent oxygen sensors. Macromolecules 34 (6), 1917–1927. doi:10.1021/ma001454j.

Maybeck, P.S., 1982. Stochastic Models, Estimation, and Control. Academic Press, New York, NY.

Merkel, T.C., Bondar, V., Nagai, K., Freeman, B.D., 2000. Sorption and transport of hydrocarbon and perfluorocarbon gases in poly(1-trimethylsilyl-1-propyne). J. Polym. Sci. Pol. Phys. 38 (2), 273–296. doi:10.1002/(SICI)1099-0488(20000115)38:2<273::AID-POLB1>3.0.CO;2-X.

Nagy, Z.K., Braatz, R.D., 2010. Nonlinear model predictive control for batch processes. In: Levine, W.S. (Ed.), The Control Handbook: Control Systems Applications, second ed. CRC Press, Boca Raton, Florida, pp. 15.1–15.30.

Ramkrishna, D., Amundson, N.R., 1974. Transport in composite materials: Reduction to a self adjoint formalism. Chem. Eng. Sci. 29 (6), 1457–1464. doi:10.1016/0009-2509(74)80170-3.

Rani, K.Y., Rao, V.S.R., 1999. Control of fermenters–a review. Bioprocess Eng. 21 (1), 77–88. doi:10.1007/PL00009066.

Rosenbluth, M.N., Berk, H.L., Doxas, I., Horton, W., 1987. Effective diffusion in laminar convective flows. Phys. Fluids 30 (9), 2636–2647. doi:10.1063/1.866107.

Sagues, F., Horsthemke, W., 1986. Diffusive transport in spatially periodic hydrodynamic flows. Phys. Rev. A 34 (5), 4136–4143. doi:10.1103/PhysRevA.34.4136.

Saha, P., Patwardhan, S., Ramachandra Rao, V., 1999. Maximizing productivity of a continuous fermenter using nonlinear adaptive optimizing control. Bioprocess Eng. 20 (1), 15–21. doi:10.1007/s004490050553.

Simon, L., Karim, M.N., 2002. Control of starvation-induced apoptosis in Chinese hamster ovary cell cultures. Biotechnol. Bioeng. 78 (6), 645–657. doi:10.1002/bit.10250.

St-Denis, C.E., Fell, C.J.D., 1971. Diffusivity of oxygen in water. Can. J. Chem. Eng. 49 (6). doi:10.1002/cjce.5450490632. 885–885

Szita, N., Boccazzi, P., Zhang, Z., Boyle, P., Sinskey, A.J., Jensen, K.F., 2005. Development of a multiplexed microbioreactor system for high-throughput bioprocessing. Lab Chip 5 (8), 819–826. doi:10.1039/B504243G.

Valappil, J., Georgakis, C., 2000. Systematic estimation of state noise statistics for extended Kalman filters. AIChE J. 46 (2), 292–308. doi:10.1002/aic.690460209.

Yoo, S.J., Jeong, D.H., Kim, J.H., Lee, J.M., 2016. Optimization of microalgal photobioreactor system using model predictive control with experimental validation. Bioproc. Biosyst. Eng. 39 (8), 1235–1246. doi:10.1007/s00449-016-1602-0.

Zanzotto, A., Szita, N., Boccazzi, P., Lessard, P., Sinskey, A.J., Jensen, K.F., 2004. Membrane-aerated microbioreactor for high-throughput bioprocessing. Biotechnol. Bioeng. 87 (2), 243–254. doi:10.1002/bit.20140.

Zhang, Z., Boccazzi, P., Choi, H.-G., Perozziello, G., Sinskey, A.J., Jensen, K.F., 2006. Microchemostat–microbial continuous culture in a polymer-based, instrumented microbioreactor. Lab Chip 6 (7), 906–913. doi:10.1039/B518396K.